Using the SpectraCube to Build a Multispectral Image Database

Graham D. Finlayson, Steven D. Hordley, Peter Morovic
School of Computing Sciences, University of East Anglia
NR4 7TJ Norwich, United Kingdom

Abstract

Multispectral image capture, unlike traditional RGB imaging, records the colour signals in a scene. Most available devices are either filter-wheel multiple exposure systems or point-measuring diffraction grating based devices. In this article we introduce a 2D matrix, full spectral, single exposure capture system – the Applied Spectral Imaging SpectraCube – which determines multispectral images, building on on the principle of interferometry.

We explain the theory of operation of the SpectraCube, show characterisation results and present an initial multispectral database of indoor images. This step is not trivial. Often there are significant errors in the spectra captured by the SpectraCube. However, these errors are surprisingly regular and can be corrected. The images were captured at a high spectral resolution, comparable to spectroradiometers, yet at an exposure significantly shorter than that of filter-wheel based systems.

1. Introduction

Traditional image capture techniques employed in most digital colour input devices are limited by the spectral sensitivity properties of the device. Since such devices are in general not colorimetric, this limits the accuracy of capture and consequently the accuracy of reproduction.

In multi-spectral imaging instead of coarsely sampling the colour signal through three filters, the signal is sampled more finely. This has the advantage of enabling spectral reconstruction of the entire scene, which in turn facilitates more accurate reproduction. Furthermore, being able to capture a scene as a matrix of colour signals instead of a matrix of RGBs, also helps for example in identifying colourants used in fine art [10], colorimetric imaging[5], the design of spectral sensitivities [17] and in other applications.

One approach to capturing multispectral images is to use multiple filters where, instead of the standard three filters, a set of filters are used [12, 7]. While this method enables a 2D capture of sampled colour signals, multiple sequential exposures are required. As a consequence exposures are very long (e.g. on the order of 5 minutes[15]). Also, spectral resolution of these systems is low; the number of filters ranges between six to at most 31 (using Liquid Crystal Tunable Filters). Consequently the captured images need to be processed using spectral reconstruction techniques to arrive at an approximation of the colour signal at each pixel.

A high accuracy alternative to filter based systems are spectroradiometers. The colour signal passes through the shutter of this device, is directed to a concave diffraction grating which breaks up the signal into its constituent parts and focuses the diffracted signal onto a photo-sensitive array[14]. The spectral resolution, stability and accuracy of such devices is very high. For example the Photoresearch PR650 measures light from 380 to 780 nm at a 4nm sampling rate, resulting in 101 samples (compared to 6 to 31 above). The disadvantage of such devices is however that they only measure a single point and are therefore impossible to use for full scene capture.

In this paper we consider a new device that addresses both the shortcoming of low spectral resolution and long exposure in filter based systems and the inability to capture full scenes using a spectroradiometer. Based on the (more than 100 year old) idea of Lippmann photography[9], the *Applied Spectral Imaging SpectraCube* is an interferometry based digital camera. This device uses the idea that if interference of the colour signal is created and measured, the spectrum of the original signal can be recovered using the inverse Fourier Transform[13].

The SpectraCube is a portable digital camera. Like a filter based system, a full 2D array of spectra is captured at once. However, unlike filter based systems, a single exposure is taken. While this single exposure is comparatively long with respect to standard RGB photography, it usually ranges from 30 seconds to a approximately 150 seconds (depending on spatial and spectral resolution and aperture). Moreover, because of the principle of operation, spectral resolution can be set to be much higher than most filter based systems.

So far, the SpectraCube has only been used in the area of microscopy[1]. In this paper we introduce the SpectraCube to the field of colour imaging. We describe it's theory of operation in some detail and examine how it's

accuracy compares to a diffraction grating based spectroradiometer. We derive a characterisation transform that accounts for a large proportion of the discrepancy between these two devices and achieve good accuracy. We then present an initial multi-spectral image database of indoor scenes.

2. SpectraCube Theory of Operation

In this section we look at the physics of *interferometry*, the principle based on which the SpectraCube captures multi-spectral images. We define light as an electromagnetic wave, and derive the interference of two such waves. We then describe methods to create and measure interference. Finally we show how measuring the interference of a signal and it's phase-shifted equivalent is used to arrive at the spectral power distribution of the colour signal.

Let us start by considering two equivalent electromagnetic waves *in vacuo* that originate from a single point source, and travel paths of different lengths. Since the two waves come from the same source, they have the same frequency ϕ and the same amplitude $\mathbf{E_0}$. The two wave equations are written as [13]:

$$\mathbf{E_1} = \mathbf{E_0}\cos(\omega\mathbf{x_1} - \phi\mathbf{t}) \quad (1)$$

$$\mathbf{E_2} = \mathbf{E_0}\cos(\omega\mathbf{x_2} - \phi\mathbf{t}) \quad (2)$$

where ω is the wave-number (the reciprocal of wavelength: $\omega = 1/\lambda$, where λ denotes wavelength), x_1 and x_2 the lengths of the paths that each wave travel and t denotes time.

Interference occurs when two electromagnetic waves combine. It can be either constructive (enhancing), if the resulting electromagnetic wave has bigger peaks than either of the signals (the waves are in phase), or destructive (diminutive) if the resulting electromagnetic wave has smaller peaks than either of the signals (the waves are out of phase). According to the principle of superposition, the two waves in Eqs. (1) and (2) reunite and result in a new electromagnetic wave given by $\mathbf{E} = \mathbf{E_1} + \mathbf{E_2}$, with a corresponding radiant power density I given by $I = \langle\mathbf{E^2}\rangle$ where $\langle\cdot\rangle$ denotes time average. Substituting for $\mathbf{E}$ and simplifying we arrive at:

$$I = \langle\mathbf{E_1^2} + \mathbf{E_2^2} + \mathbf{2E_1}\cdot\mathbf{E_2}\rangle \quad (3)$$

We can also write the above in terms of the respective radiant power densities of the two waves as $I = I_1 + I_2 + I_{12}$. Interference occurs if the *interference term* I_{12} is non-zero. This is the case if the dot-product of $\mathbf{E_1}$ and $\mathbf{E_2}$ is non-zero and is maximal (minimal) when these vectors are parallel (orthogonal). Let us further consider only the term $I_{12} = 2\langle\mathbf{E_1}\cdot\mathbf{E_2}\rangle$. Their inner dot-product can be written as:

$$\mathbf{E_1}\cdot\mathbf{E_2} = \mathbf{E_0}\cdot\mathbf{E_0}\cos(\omega\mathbf{x_1} - \phi\mathbf{t})\cos(\omega\mathbf{x_2} - \phi\mathbf{t}) \quad (4)$$

Expanding the cosine factors, denoting $\delta = x_1 - x_2$ the optical path difference of the two waves and simplifying we arrive at [3]:

$$\mathbf{E_1}\cdot\mathbf{E_2} = \frac{\mathbf{1}}{\mathbf{2}}\mathbf{E_0^2}\cos(\omega\delta) \quad (5)$$

and likewise we arrive at irradiance (as a function of δ) as $I = 2S(\omega)(1 + \cos\omega\delta)$, where $S(\omega)$ denotes the spectral distribution of the source (equivalent to both I_1 and I_2, since the source is the same).

To create as well as quantify interference under controlled conditions, an interferometer is used. This is an optical device that measures the interference pattern of two electromagnetic waves (originating from the same source) in some defined wavelength interval.

The classical design is that of the Michelson Interferometer [13] (see Fig. 1). In this design, the signal that enters the device falls on a beam splitter. Half the amplitude of the signal is let through the beam splitter and falls on a fixed mirror, the other half is reflected perpendicularly to another mirror that varies it's distance to the beam splitter. Both mirrors reflect the respective signals impinging on them and through the beam splitter they are reunited. Since the two signals differ in the length of the path they travelled, a phase shift in the wave occurs, which results in interference. By varying the difference in the length of the path, a function of the optical path difference (OPD) δ can be measured. This function is referred to as the *interferogram* and can be shown to be the inverse Fourier Transform of the spectrum of the signal [2].

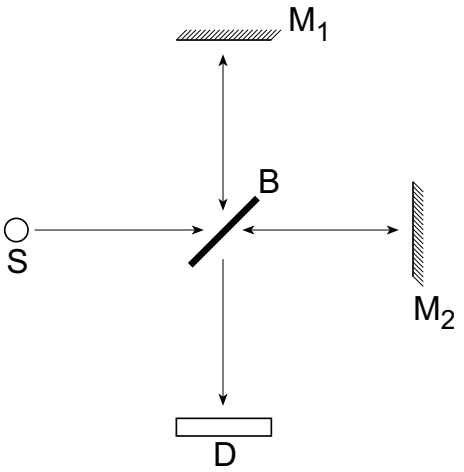

Figure 1: *Diagram of the Michelson Interferometer. S - source, M1 - first mirror, M2 - second mirror, B - beam splitter, D - detector.*

The interference of two identical electromagnetic waves described by a common spectral irradiance distribution $S(\omega)$, reuniting after a path difference of δ is $I = 2S(\omega)(1 +$

$\cos\omega\delta)$. Since the source will contain energy at many wavenumbers ω, I can be interpreted as irradiance per unit ω interval at ω, giving an integrated radiant power density over all wavenumbers, as a function of δ:

$$\begin{aligned} I(\delta) &= \int_0^\infty 2S(\omega)(1+\cos\omega\delta)d\omega = \\ &= \int_0^\infty 2S(\omega)d\omega + \int_0^\infty 2S(\omega)\cos\omega\delta d\omega \quad (6) \end{aligned}$$

The first integral is a constant term and does not depend on δ, while the second integral represents interference between the two waves and can be interpreted as a positive or negative deviation from the constant term, as a function of the path difference δ. Irradiance fluctuations about the constant term describe the interferogram given by the second integral term:

$$I(\delta) = \int_0^\infty 2S(\omega)\cos\omega\delta d\omega \quad (7)$$

If the spectrum is monochromatic, peaking at ω_i, then the interferogram is a sinusoid of constant amplitude $2S(\omega_i)$. However, if the spectrum is a broadband source, the interferogram becomes a sinusoid with periodically varying amplitude (see Fig. 2).

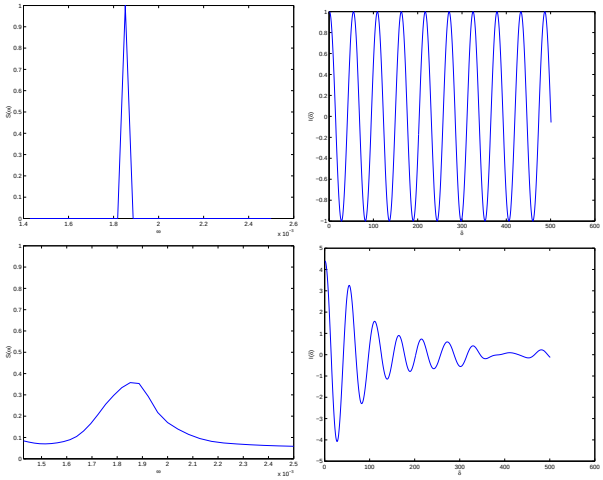

Figure 2: *Spectrum and interferogram of a monochromatic light source (top left and top right); spectrum and interferogram of a broad band light source (bottom left and bottom right).*

The interferogram $I(\delta)$ depends on the spectrum $S(\omega)$ according to a cosine Fourier integral. Following the inversion theorem that can be applied to this type of integral[2], we arrive at the spectral power distribution of the original source as:

$$S(\omega) = \int_0^\infty I(\delta)\cos\omega\delta\ d\omega \quad (8)$$

Thus, by measuring the interferogram $I(\delta)$ and applying an inverse Fourier Transform, we are able to recover the sought spectral power distribution of the light $S(\omega)$.

The Applied Spectral Imaging (ASI) SpectraCube is an interferometry based spectroradiometer (spectroscope or high-resolution multi-spectral camera). In particular it uses the rotating Sagnac Interferometer design [8] similar in principle to the Michelson Interferometer described earlier. In this type of interferometer, the two signals that are created after the original signal passes through the beamsplitter, travel the same optical path, however in opposing directions. Once the signals are recombined, they create interference patterns measured by a light sensitivite charge coupled device (CCD)[8].

3. Applied Spectral Imaging© SpectraCube

The Applied Spectral Imaging SpectraCube (SP3) allows for a variety of settings depending on the captured scene, required spatial and spectral resolution and signal to noise ratio. It is possible to measure spectra in the interval of 300nm and 1100nm, or any single continuous sub-interval. Due to the nature of the device, spectral sampling is non-uniform. The shorter the wavelengths the higher the frequency of sampling, and vice versa the longer the wavelengths the fewer samples are taken. The spatial resolution of the CCD is 1024 by 1024 pixels, however capture of any sub-rectangle (region of interest) is possible.

The spectral resolution is chosen indirectly through the *number of frames* (NoF) and *interferometer steps between frames* (ISF). The NoF is the number of measurement points in the interferogram, while the ISF is the distance the interferometer travels between frames[16]. The spectral resolution is then determined by the product of NoF and ISF. This product is the total distance the intereferometer travels during acquisition. As this product is increased a longer part of the interferogram is sampled. The longer the interferogram, the higher the spectral resolution of the captured spectrum.

To increase the signal to noise ratio (SNR) there are two possibilities, increasing exposure of each frame (not exceeding saturation), or increasing the NoF while keeping the spectral resolution the same. To do the latter, as the NoF is increased, so the ISF is decreased.

Spectral and spatial resolution, signal to noise ratio (determined by the relation of NoF and ISF), exposure and memory requirements are closely linked. The higher the spectral or spatial resolution or signal to noise ratio, the more memory is required and the longer the exposure of the scene. Thus low spectral resolution, full frame images at a medium to high signal to noise ratio setting can be taken at a relatively short exposure (approximately 30 seconds), while maximum spectral resolution full frame

images at the highest signal to noise ratio would require several minutes and several gigabytes of memory to capture.

4. SpectraCube Characterisation

The principle of operation of the SP3 camera is different from other devices used in colour imaging. In this section we look at the correspondence of the SP3 compared to another device. In order to characterise the SP3 camera, we compare it to a point-measuring telespectroradiometer, the PhotoResearch PR650. Let us first describe the PR650 and compare it to the SP3 camera.

The PR650 is a diffraction grating based telespectroradiometer measuring the spectrum of a single point in a scene, an average over a small central circular area of the lens, from 380nm to 780nm at uniform 4nm sampling intervals, resulting in a 101 dimensional spectrum vector. Exposure is set automatically by the device, and varies from measurement to measurement, therefore varying with a different light source / intensity / sample. Implicitly we consider the PhotoResearch PR650 to be the ground truth.

Earlier we have described in some detail the SpectraCube. This device has variable spectral resolution. Since illuminants used in this study include fluorescents, it is important to have a high spectral sampling frequency to account for peaks that are characteristic for such light sources. This has a consequence of relatively long exposure. Also, the SP3 sets exposure globally for the entire scene, rather than individually for each patch as is the case with the PR650. The settings used for the SP3 are such that the maximum sampling step is no more than approximately 10nm.

The characterisation was based on the Macbeth Digital ColorChecker Chart (MBDC). This calibration chart has 12 rows and 20 columns of paper patches of which 8 are glossy and the remainder matte. The first and the last row and column of the chart are composed of alternating white, grey and black patches, these were not included in the measurements, as they do not increase the dimensionality of the data. Thus we use 180 patches of the 240 patch chart. The MBDC was taken under five different light sources in a VeriVide viewing booth, four fluorescents (daylight simmulators D50 and D75, cool white fluorescent and TL84) and Tungsten lightbulbs (illuminant A).

Measuring the MBDC with the PR650 results in a matrix of 180 vectors of 101 samples. Since the SP3 measures an entire image, the entire MBDC has been captured and then, averaging 4 pixels (a 2 by 2 square) in the centre of each of the 180 patches, reduced to a set of 180 spectra. The SP3 set of spectra is interpolated to the spectral range of the PR650 (380nm to 780nm at a sampling rate of 4nm). Thus, for comparison, we start with two 101×180 matrices. Due to differences in exposure, we furthermore normalise the two sets such that the central white patch of the MBDC has a spectrum summing to one.

The characterisation error is expressed in terms of three error measures. We examine the angular difference between two XYZs corresponding to spectra from the two devices, the standard CIE LAB ΔE colour difference measure between corresponding CIE Lab values of the spectra [6] and finally the relative root-mean-square (RMS) difference of the spectra themselves.

Let us denote $\mathbf{A}$ the 101×180 matrix of 180 spectra A_i taken with the SP3 and $\mathbf{B}$ the 101×180 matrix of the 180 corresponding spectra B_i measured with the PR650. Angular difference between two XYZs K_i and L_i corresponding to these vectors is expressed as:

$$\text{ANGe}_i = \frac{\cos^{-1}(K_i \cdot L_i)}{\sqrt{K_i \cdot K_i}\sqrt{L_i \cdot L_i}} \tag{9}$$

where we assume angles are measured in degrees.

CIE Lab colour difference is the Euclidean distance between the Lab values corresponding to A_i and B_i[6]. RMS of a $101 \times N$ matrix $\mathbf{M}$ is defined as:

$$\mathcal{R}(\mathbf{M}) = \sqrt{\frac{\mathbf{D}(\mathbf{M^T M})}{\mathbf{101}}} \tag{10}$$

where $D()$ is a function returning the diagonal elements of a matrix. We then express relative RMS error as:

$$\text{RMSe} = \frac{\mathcal{R}(\mathbf{A} - \mathbf{B})}{\mathcal{R}(\mathbf{A})} \tag{11}$$

where RMSe here is a vector of 180 values.

Table 1 summarises the correspondence between PR650 and SP3 in terms of the mean and median of these measures over all 180 samples.

Ill	RMSe		ANGe		LABe	
	mean	med.	mean	med.	mean	med.
D50	0.329	0.333	16.25	16.34	3.13	2.52
D75	0.274	0.274	13.97	14.13	2.98	2.74
CWF	0.279	0.260	13.47	12.78	3.37	2.78
TL84	0.470	0.469	27.01	27.42	3.04	2.54
A	0.240	0.235	12.53	12.64	10.23	7.51

Table 1: *Difference between PR650 spectra and uncorrected SP3 spectra.*

The results in Table 1 show a surprisingly big discrepancy. However, when looking at the spectral difference between the two sets of data one can observe a harmonic error, in that each of the 180 difference functions shows a common pattern. We account for this by deriving an error-minimising transform that maps spectra from the SP3 to spectra from the PR650. Minimising error in the least-squares sense amounts to solving for $\mathbf{T}$ such that $\| \mathbf{AT} -$

$\mathbf{B} \parallel$ is minimal. The solution to this minimisation is found easily as $\mathbf{T} = \mathbf{A}^{+}\mathbf{B}$, where $\mathbf{A}^{+} = (\mathbf{A^T A})^{-1}\mathbf{A^T}$ is the Moore-Penrose (or pseudo) inverse. However the system we are solving is under-determined; although we have 180 spectra, they do not span 101 dimensions. In spite of the high dimensionality of the MBDC, 20 basis vectors derived by Characteristic Vector Analysis[11] cover 99.99% of variation in the data. Thus, a simple least squares matrix would be prone to noise and need not be a good fit when applied to data other than that used to derive itself (the training set). A consequence is that the condition number of $\mathbf{T}$ will be very large. It is therefore desirable to regularise this solution.

Instead of solving for the simple least squares matrix, a new optimisation is formulated as:

$$\min_{\mathbf{T}} \parallel \mathbf{AT} - \mathbf{B} \parallel_{\mathbf{2}} + \alpha \parallel \mathbf{T} \parallel_{\mathbf{2}} \qquad (12)$$

where α is a weighting factor of the norm of the sought transform. In effect we add a penalty term associated with the norm of the transform matrix. This approach is known as the Tikhonov regularisation[4]. The solution to Eq. (12) is directly derived as $\mathbf{T} = \mathbf{C}^{+}\mathbf{A^T B}$, where $\mathbf{C} = (\mathbf{A^T A} + \alpha\mathbf{I})$, such that $\mathbf{I}$ is the identity matrix[4].

Finding the weighting factor α is non-trivial. For the purpose of this work a simple routine based on Newton's iterative bisection technique was implemented to find an α that results in minimal error for a testing set.

In Table 2 we present the difference between spectra from the PR650 and spectra from the SP3 corrected using a mapping matrix $\mathbf{T}$ derived based on all data sets and tested on each data set separately. Results are presented, as before, in terms of three difference measures. Note that the measure that is optimised by Eq. (12) is the root mean square metric.

Ill	RMSe		ANGe		LABe	
	mean	med.	mean	med.	mean	med.
D50	0.029	0.021	1.27	0.99	1.23	1.03
D75	0.029	0.020	1.29	0.91	1.14	0.95
CWF	0.035	0.023	1.47	1.07	1.41	1.24
TL84	0.028	0.017	1.00	0.70	1.23	1.07
A	0.043	0.024	1.62	0.83	5.46	3.73

Table 2: *Difference between PR650 spectra and corrected SP3 spectra. The correction is derived based on all data sets.*

In Table 3 we show results when deriving the mapping based on 90 out of the 180 spectra from all sets (one per illuminant) and testing against the remaining 90 spectra from these sets. The training set is simply the set of spectra with odd indices, while the testing set is the set of spectra with even indices.

From both Table 2 and 3 we see an order of magnitude of improvement over uncorrected data in Table 1, in terms of the optimised RMSe difference measure. While results

Ill	RMSe		ANGe		LABe	
	mean	med.	mean	med.	mean	med.
D50	0.035	0.025	1.49	1.15	1.51	1.12
D75	0.033	0.022	1.40	1.00	1.59	1.12
CWF	0.042	0.026	1.70	1.16	1.86	1.46
TL84	0.035	0.019	1.26	0.85	1.65	1.17
A	0.051	0.028	1.86	0.92	7.05	4.04

Table 3: *Difference between PR650 spectra and corrected SP3 spectra. The correction is derived based on half the data (90 spectra from the full set).*

for the four fluorescent illuminants (D50, D75, CWF and TL84) are consistent throughout, illuminant A is slightly worse (both corrected and uncorrected). This is understandable as illuminant A is smooth and slowly varying, while the fluorescent illuminants have sharp peaks and a high frequency of spectral variation. Thus, the spectral resolution used to capture data under fluorescent light sources is likely to be too high for illuminant A. Also, a single mapping is derived based on five data sets, four of which are fluorescents. It follows that the matrix will be biased towards fluorescents.

5. The Multispectral Database

We present the first set of images of a new multispectral database. Initially we have taken three scenes in a viewing booth under illuminants D50, D75, CWF, TL84 and A. The aim for this database is to be a freely accessible set of spectral images. This can be used in many ways, such as sensor design, spectral analysis of surfaces, color signal estimation algorithm development, colour constancy algorithm development etc..

Images taken with the SP3 were corrected, based on the characterisation developed earlier in Section 4. Such that images taken under illuminant D50, were corrected using a mapping matrix derived from the Macbeth Digital ColorChecker taken under the same light source. While our experimental results presented in the previous section are encouraging, we are currently evaluating the accuracy of this characterisation applied to these images. All images from are available at
www.cmp.uea.ac.uk/pm/multispectral.html.

Figure 3 shows a sub-set of 9 frames from the spectral capture using the SP3 of the 'cereals' image.

6. Conclusions

In this paper we described an interferometry based multispectral digital camera, the ASI SpectraCube. We looked at it's precision and derived a characterisation matrix. We presented an initial multi-spectral dataset for colour research.

The main advantages of the SpectraCube over previous devices is: it measures a 2D matrix of spectra, rather than a single point; it has considerably shorter exposure times compared to filter-wheel based set-ups; it is transportable, unlike most other systems; it enables the adjustment of spectral and spatial resolution; has high spectral range (300 nm to 1100 nm).

References

[1] D. Cabib, R. A. Buckwald, Yuval Garini, and Dirk G. Soensken. Spatially resolved fourier transform spectroscopy (spectral imaging): A powerful tool for quantitative analytical microscopy. *SPIE*, 2678:278 – 291, 1996.

[2] John Chamberlain. *The Principles of Interferometric Spectroscopy*. John Wiley & Sons, 1979.

[3] M. Françon. *Optical Interferometry*. Academic Press, 1966.

[4] Gene H. Golub and Urs von Matt. Tikhonov regularization for large scale problems.

[5] Jon Yngve Hardeberg, Francis Schmitt, and Hans Brettel. Multispectral image acquisition and simulation of illuminant changes. 1999.

[6] Robert W. G. Hunt. *The Reproduction of Colour*. Fountain Press, Kingston-upon-Thames, England, 1995.

[7] Francisco H. Imai, Mitchell R. Rosen, and Roy S. Berns. Comparison of spectrally narrow band capture versus wide band with a priori sample analysis for spectral reflectance estimation. 2000.

[8] Moshe Lavi, Uri Milman, Dario Cabib, Yuval Garini, Amir Gil, Ton Juta, and Mike Adel. A new compact design interferometer based spectral imaging system for bio-medical applications. *SPIE*, 3261:313 – 321, 1998.

[9] Gabriel Lippmann. Sur la theorie de la photographie des couleurs simples et composees par la methode interferentielle. *J. Physique*, 3(3):97 – 107, 1894.

[10] Henri Maitre, Francis Schmitt, Jean-Pierre Crettez, Yifeng Wu, and Jon Yngve Hardeberg. Spectrophotometric image analysis of fine art paintings.

[11] Lawrence T. Maloney. Evaluation of linear models of surface spectral reflectance with small numbers of parameters. *Journal of the Optical Society of America A*, 3(10):1673–1683, October 1986.

[12] Kirk Martinez, David Saunders, and John Cupitt. High-resolution colorimetric imaging of paintings. pages 25 – 36, 1993.

[13] Frank L. Pedrotti and Leno S. Pedrotti. *Introduction to Optics*. Prentice-Hall International, 1996.

[14] Photo Research. *PR-650 SpectraScan SpectraColorimeter Instruction Manual*. Photo Research, Inc., 1999.

[15] Mitchell R. Rosen and Xiao-Yun (Willie) Jiang. Lippmann2000: A spectral image database under construction. 1999.

[16] Applied Spectral Imaging. *Spectral Imaging 2.6: Spectral Imaging Acquisition Software Manual*. Applied Spectral Imaging, 2001.

[17] Poorvi L. Vora, Joyce E. Farrell, Jerome D. Tietz, and David H. Brainard. Image capture: Simulation of sensor responses from hyperspectral images. *IEEE Transactions on Image Processing*, 10(2):307 – 315, 2001.

Figure 3: *Intensity images at 9 wavelengths from 400 to 700 nm).*